Chapter-4

Fabrication and Characterization of High-Performance ZnO CQDs/ $MoSe_2$ Heterojunction UV-Visible Broadband Photodetector

The Part of the work is adopted from-

S. Singh, A. P. Singh and S. Jit, **"High Performance ZnO CQDs/$MoSe_2$ Heterojunction UV-Visible Broadband Photodetector," in *IEEE Photonics Technology Letters*,** vol. 37, no. 4, pp. 247-250, 15 Feb.15, 2025, doi: 10.1109/LPT.2025.3535626.

4.1 Introduction

Zinc Oxide (ZnO) nanostructures have been widely investigated for ultraviolet (UV) detection applications due to their high surface-to-volume ratio, wide direct bandgap (~3.37 eV), excellent thermal and chemical stability, and environmentally friendly nature [6], [8], [58], [93]. Owing to its low cost and abundant availability, ZnO is considered a potential alternative to the more expensive GaN for UV optoelectronic applications, as both materials exhibit similar electronic and optoelectronic properties. This has encouraged researchers to explore heterostructures composed of transition metal dichalcogenides (TMDs) and ZnO nanostructures to achieve enhanced photoresponse across the UV to visible spectral range, driven by their synergistic optoelectronic interactions [42], [51].

TMD/ZnO nanostructure architectures benefit from the broad spectral sensitivity of ZnO and the high carrier mobility and atomic thickness of TMDs, which collectively facilitate efficient photocarrier separation and signal amplification. For instance, Kang et al. demonstrated flexible photodetectors using atomic layer deposition (ALD) of ZnO nanopatches on MoS_2 nanosheets, achieving a responsivity of approximately 2.7 A/W under visible light illumination [92]. Zheng et al. reported a WS_2/ZnO quantum dot (QD) heterojunction exhibiting an outstanding responsivity of ~1120 A/W, detectivity of 3.2×10^{12} Jones, and an ultrafast response time of ~15 ns [109]. Nazir et al. [110] developed a ZnO QD-decorated MoS_2 thin film photodetector with significantly enhanced photoresponse characteristics. A type-I heterostructure of ZnO QDs and MoS_2 monolayer for UV-visible photodetection was reported by Zhou et al. [97]. Additionally, Putri et al. [111] demonstrated a UV photodetector

based on $MoSe_2$ quantum dots decorated onto ZnO nanostructures, while Wan et al. [58] introduced a self-powered broadband photodetector using a $MoSe_2$/ZnO heterojunction. Since $MoSe_2$ remains a relatively underexplored TMD material, there exists considerable potential for further exploration of $MoSe_2$/ZnO nanostructures in broadband photodetection applications.

This chapter focuses on the performance investigation of an Ag/n-$MoSe_2$/n-ZnO colloidal quantum dots (CQDs)/ITO-based broadband UV-visible photodetector operating in the 300–700 nm wavelength range. ZnO CQD thin films were synthesized using the conventional hot injection method [8], [101] and deposited on ITO-coated glass substrates via the spin-coating technique as described in Chapter 1. $MoSe_2$ nanopowder, synthesized hydrothermally, was subsequently deposited on the ZnO CQD layer through vacuum thermal evaporation, as detailed in earlier chapters. The proposed photodetector demonstrated a maximum responsivity (R) of ~282 A/W, detectivity (D) of ~9×10^{12} Jones, and an external quantum efficiency (EQE) of ~90,000% at 380 nm (under an incident light intensity of 47 $\mu W/cm^2$) in the UV region. In the visible region, the device achieved R ≈ 16.15 A/W, D ≈ 5.37×10^{11} Jones, and EQE ≈ 3660% at 550 nm (with an incident intensity of 0.22 mW/cm^2), under an applied bias of 2 V. The organization of this chapter is outlined as follows:

Section 4.2 presents the device fabrication details, including the synthesis and deposition of ZnO CQDs and $MoSe_2$ materials. In Section 4.3, various results from thin-film characterization and optical measurements of the proposed photodetector are discussed. Finally, the summary and conclusions of this chapter are provided in Section 4.4.

4.2 Experimental Details

4.2.1. Material Preparation

All the materials and chemicals were provided from Sigma-Aldrich, USA. As the chemicals purchased were of standard purity grade, therefore, no further processing was done before utilizing it for material synthesis and device fabrication. The hot injection route was adopted for ZnO CQDs synthesis [4], [8] and hydro-thermal route was used for $MoSe_2$ nano-powder synthesis [50], [68]. For ZnO CQDs synthesis, zinc-acetate dihydrate (500 mM) was mixed in a 20ml solution of ethylene glycol monomethyl ether in a well-cleaned three-neck flask under N_2 environment. The resultant solution was continuously stirred at 800 rpm and as it turns milky, quick injection of MEA (equi-molar concentration) was done in the solution. In this complete process flask temperature was maintained at 60℃. When solution turns transparent after few minutes, temperature was suddenly dropped to stop nucleation of ZnO nanoparticles. Now, under N_2 environment the resultant solution was subjected to continuous stirring at 800 rpm for 24 h at room temperature. Finally, a syringe filter of 0.22-µm membrane was used in order to filter out the solution[4], [8]. Now, ZnO CQDs can be used for its thin-film preparation through spin-coating method.

For $MoSe_2$ nano-powder synthesis, a 60 ml ethanol: DI (1:1) solution was prepared in which selenium powder, sodium molybdate dehydrate, and sodium borohydride were added in stoichiometric ratio followed by 15 min rigorous stirring. Then, the prepared solution was poured into a well cleaned Teflon-lined stainless steel autoclave. Next, we placed the sealed autoclave in an oven at 200℃ for 48hrs. After the natural cooling of the autoclave, black

coloured precipitate was collected using centrifuge process followed by subsequent washing in ethanol and DI water for 3-5 times. At last, $MoSe_2$ nano-powder was obtained after final annealing at 60℃ for 12 hrs [50], [68]. Now, it is ready for its thin film deposition through thermal evaporation technique.

4.2.2. Device Fabrication

The ITO coated glass substrates (15 mm ×15 mm) were ultra-sonicated sequentially in soap solution, DI water, Acetone and Isopropanol for 15 min each. They were then cleaned by DI water followed by drying and plasma cleaning (Femto Science Inc., CUTE, South Korea) for 15 min in Ar:O_2 (50:50) ambient. The ZnO CQDs film was then grown on the cleaned ITO by spin coating method at 2000 rpm for 40s. This process was repeated 3-5 times to achieve thickness of ~170 nm (measured by FILMETRICS F-20 thin-film analyzer, USA). After each spin coating step, the film was heated at 120℃ for 10 min. The final film was annealed at 450℃ on a hot plate in ambient environment [8], [63]. $MoSe_2$ thin film was then grown on the ZnO CQDs film by thermal evaporation (FL400 SMART COAT 3.0 A, Hind High Vacuum, India) of hydrothermally synthesized $MoSe_2$ nano-powder at a deposition rate of 1.0 Å/sec under a high vacuum level (~2.4×10^{-6} mbar). The synthesis of $MoSe_2$ by the hydrothermal method is described in our recently published works [15], [68]. Finally, ~100 nm thick pure silver (99.99%) circular metal dots of ~1.75 mm diameter (with effective area ~0.024 cm^2) were deposited upon the $MoSe_2$ film at a 0.2 Å/sec deposition rate [4], [68]. The schematic flow diagram of the device fabrication process is shown in **Figure 4.1**. The schematic device diagram and SEM image of the fabricated device is shown in the **Figure 4.2** (a) and (b) respectively.

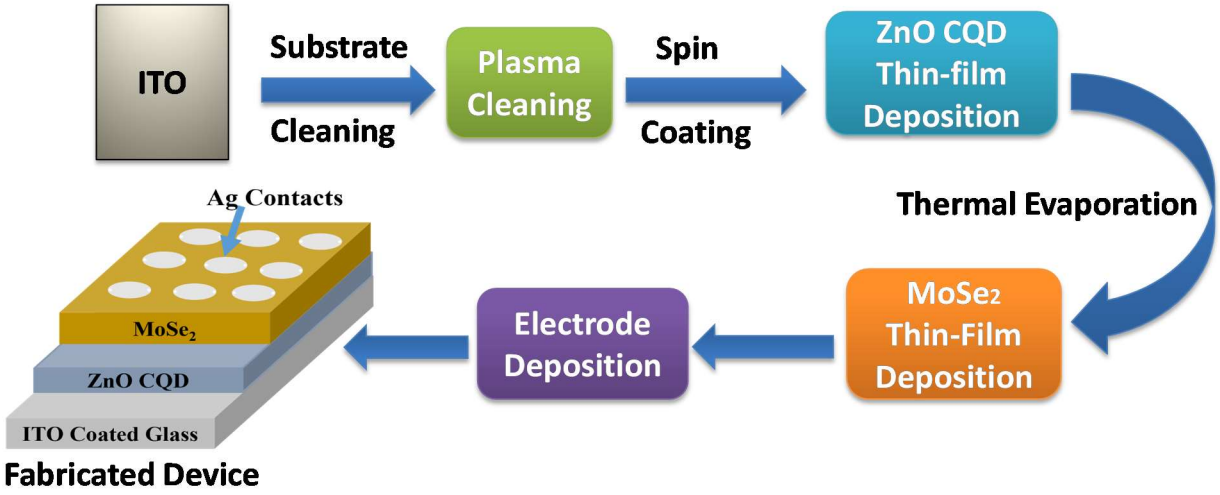

Figure 4.1 Schematic Flow Diagram of the Device Fabrication Process.

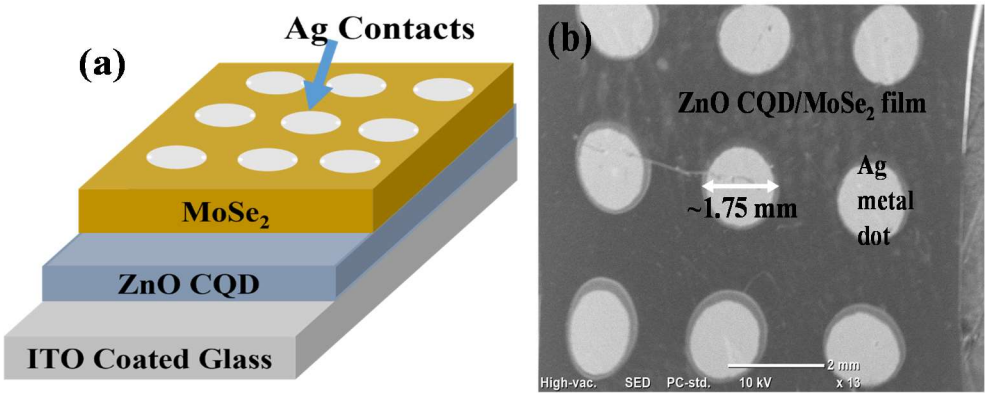

Figure 4.2 (a) Schematic device diagram; (b) SEM image of the fabricated device.

4.3. Results and Discussion

4.3.1. Optical and I-V Characterization

The characterizations of ZnO CQDs and $MoSe_2$ films are discussed in our previous chapters [4], [8], [68], [15]. The optical absorbance characteristics (measured using UV-770, JASCO, Japan) of the individual ZnO CQDs and $MoSe_2$ layers as well as their combined layer shown

in **Figure 4.3** confirm a broad absorbance spectrum (300-700 nm) of the ZnO CQDs/$MoSe_2$ heterojunction covering UV-Visible region. Absorbance in the UV region is primarily dominated by the ZnO CQDs layer while the absorbance in the visible region is dominated by the $MoSe_2$ film.

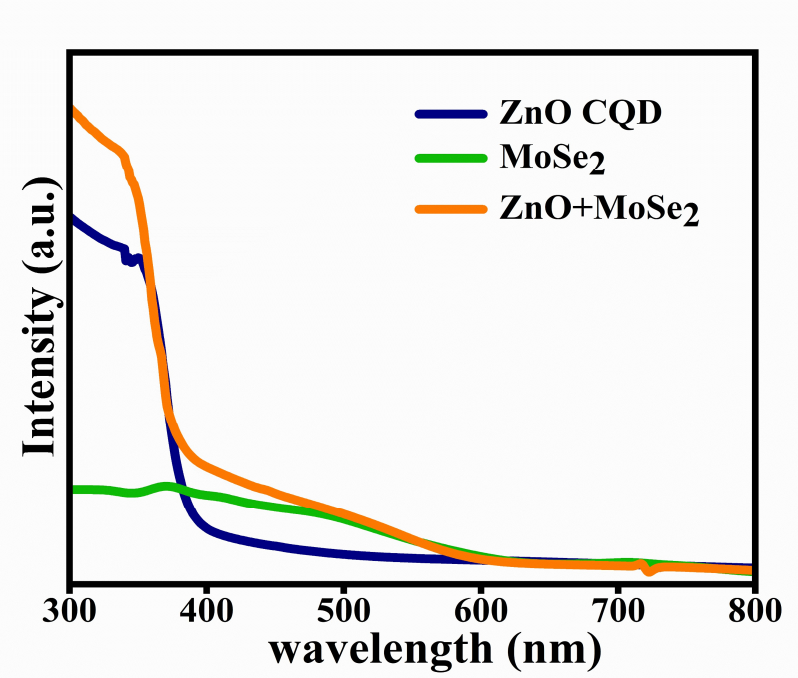

Figure 4.3 Absorbance spectrum of the fabricated device.

Figure 4.4 (a) and (b) shows the room-temperature current (I)–voltage (V) characteristics in linear and logarithmic scale respectively of the proposed ZnO CQDs/$MoSe_2$ heterostructure device measured under dark, 380 nm (with 47 $\mu W/cm^2$ intensity) and 550 nm (with 0.22 mW/cm^2 intensity) using a semiconductor parameter analyser (Model: B1500A from Keysight, USA). The nearly symmetric forward and reverse biased I-V characteristics over -2 V to 2 V confirm the formation of the n-n heterojunction under study.

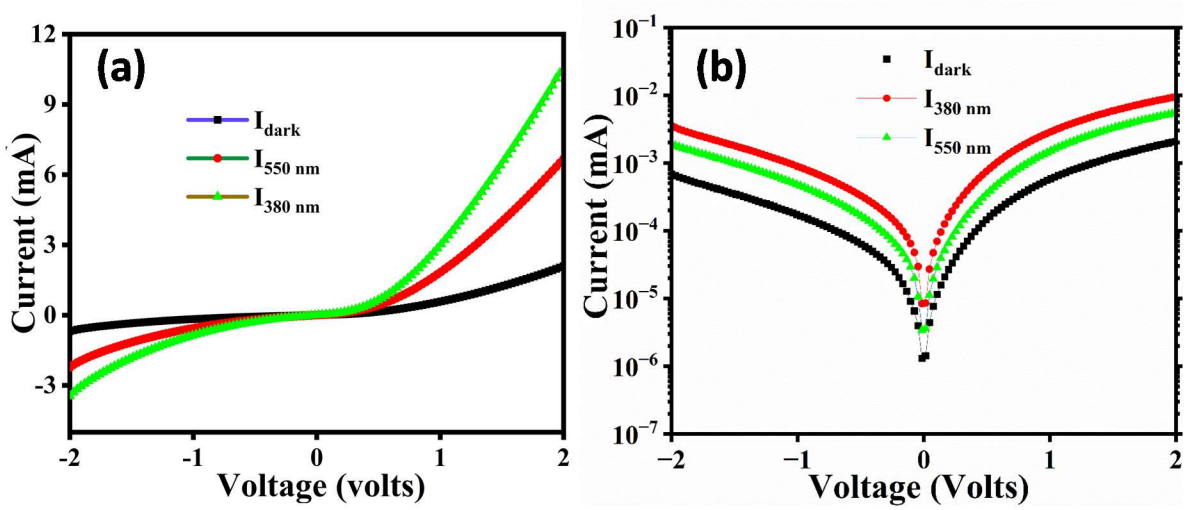

Figure 4.4 I-V characteristics (a) Linear scale (b) Logarithmic scale

4.3.2. Structural Characterization of as-grown ZnO CQDs

The transmission electron microscopy (TEM) image (TECNAI G2 20 TWIN) of the ZnO CQDs film deposited on a copper grid at 50 nm resolutions (Inset: at 20 nm resolution) is shown in the **Figure 4.5** (a). The TEM image shows the nanoparticle nature of the ZnO in the solution. The particle size distribution of the ZnO CQDs is characterized by the histogram, as shown in **Figure 4.5** (b).The histogram shows an average particle size of ZnO CQDs as 2.30 nm which is below the Bohr's radius value of 2.87 nm of the ZnO hence, confirms the QDs nature of ZnO nanoparticles in the ZnO solution prepared by the hot injection method.

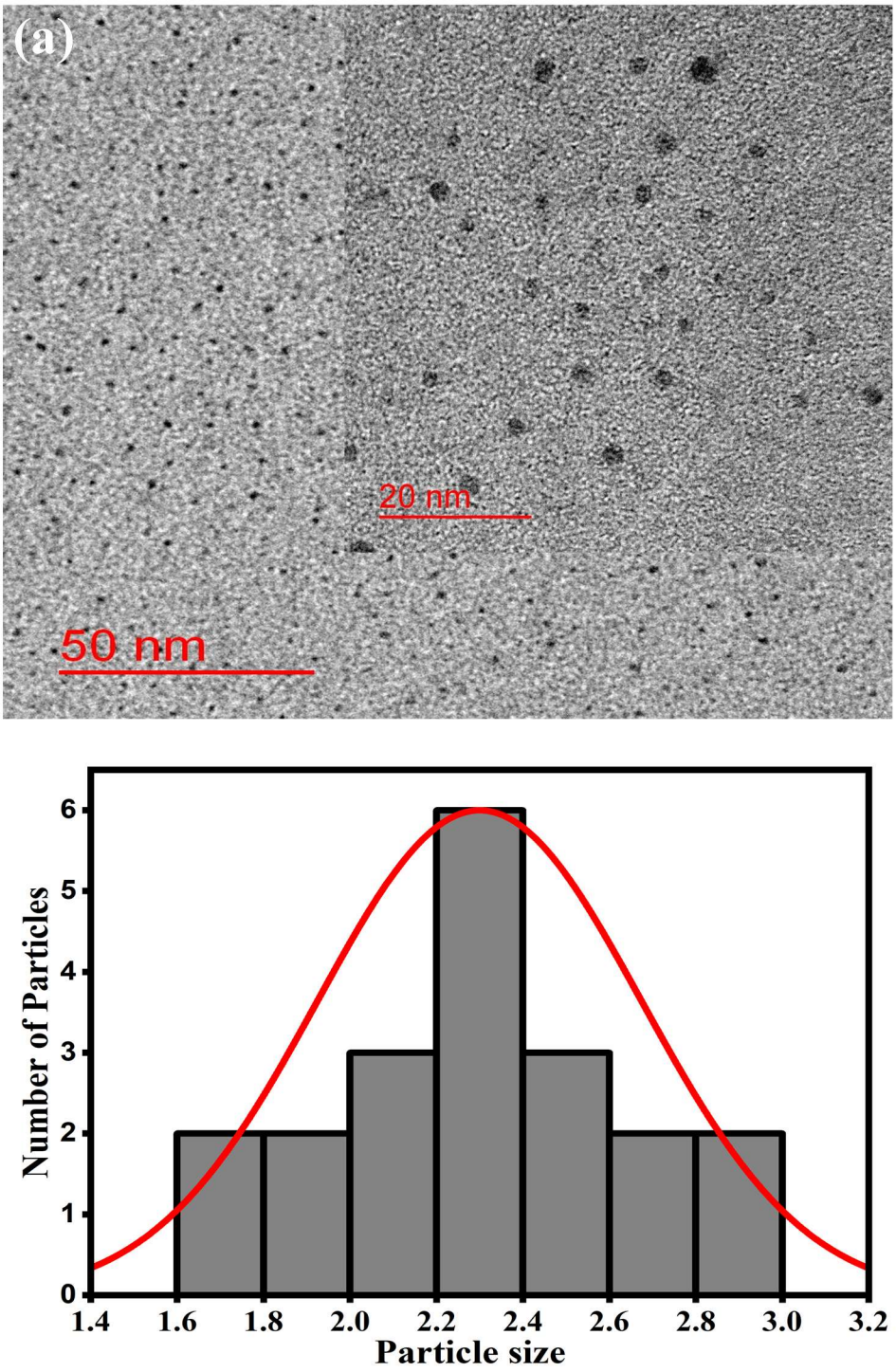

Figure 4.5 (a) TEM image of ZnO CQDs at 50 nm resolution (Inset: at 20 nm resolution); (b) Histogram of the ZnO CQDs.

4.3.3. Optoelectronic Characterization of the Fabricated Device

The basic performance parameters namely responsivity *R(λ)*, specific detectivity D^* *(λ)* and EQE (%) of the proposed n-n heterostructure device were measured at room temperature using a monochromator (SP2150i from Princeton Instruments, USA) setup with a halogen lamp as the light source. The above parameters can be defined as follows[8], [72], [73], [74]:

$$R = \frac{I_{ph}}{P_{opt}} \quad \text{A/W} \tag{4.1}$$

$$D^* = R \times \sqrt{\frac{A}{2 \times e \times I_{dark}}} \quad \text{Jones} \tag{4.2}$$

$$\text{EQE (\%)} = 1240 * \frac{R(\lambda)}{\lambda} * 100 \tag{4.3}$$

where I_{ph} is the photocurrent; P_{opt} is the incident optical power on the device; e is the charge of an electron; A is the effective area (0.024 cm^2) of the device; I_{dark} is the dark current and λ is the wavelength of the light incident on the device. **Figure 4.6**, **Figure 4.7** and **Figure 4.8** shows the responsivity, specific detectivity and EQE of the ZnO CQDs/$MoSe_2$ heterojunction device under study respectively. The maximum values of R, D* and EQE are ~282 A/W, ~9×10^{12} Jones and ~90000% respectively at 380 nm in the UV region while their corresponding maximum values at 550 nm in the visible region are ~16.15 A/W, ~5.37×10^{11} Jones and ~3660% under the applied bias voltage of 2 V. Our results are compared with other ZnO/TMD based devices in **Table 4.1**. The performance parameters of our device in the UV region much better than those reported by Putri et al. [71] for their ZnO/$MoSe_2$ and ZnO

Nanorod (NR)/$MoSe_2$ QDs heterostructure UV detectors. Especially, our extremely high EQE (of 90000%) at 380 nm in the UV region is nearly 180 times higher than the EQE (504% at 365 nm) reported for the ZnO Nanorod (NR)/$MoSe_2$ QDs device heterostructure device [71]. The high EQE beyond 100% is attributed to the trap-assisted photomultiplication (PM) phenomenon. It occurs when the photogenerated holes or electrons are trapped or blocked in the active layers, while opposite charge carriers continually pass through the active layer and are collected by the corresponding electrode. Under the reverse bias operation, photogenerated excitons will be dissociated into free charge carriers at ZnO QDs/$MoSe_2$ interface. A part of the photogenerated electrons are trapped in the ZnO QDs near the ITO electrode (cathode). The trapped electrons in ZnO QDs near the ITO electrode create a Columbic force, which induces interfacial band bending for hole injection via ITO electrode under reverse bias operation. The injected holes enhance photocurrent in the device [2], [16], [20]. Furthermore, the surface-to-volume ratio in nanomaterials is much higher than in bulk materials, which enhances the effect of photomultiplication in the device.

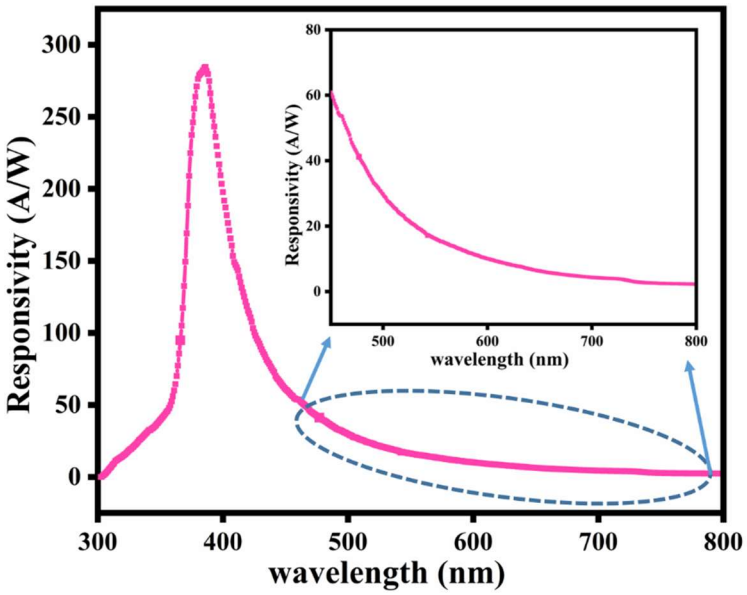

Figure 4.6 Responsivity of the Fabricated Device (Inset shows enhanced performance in visible region)

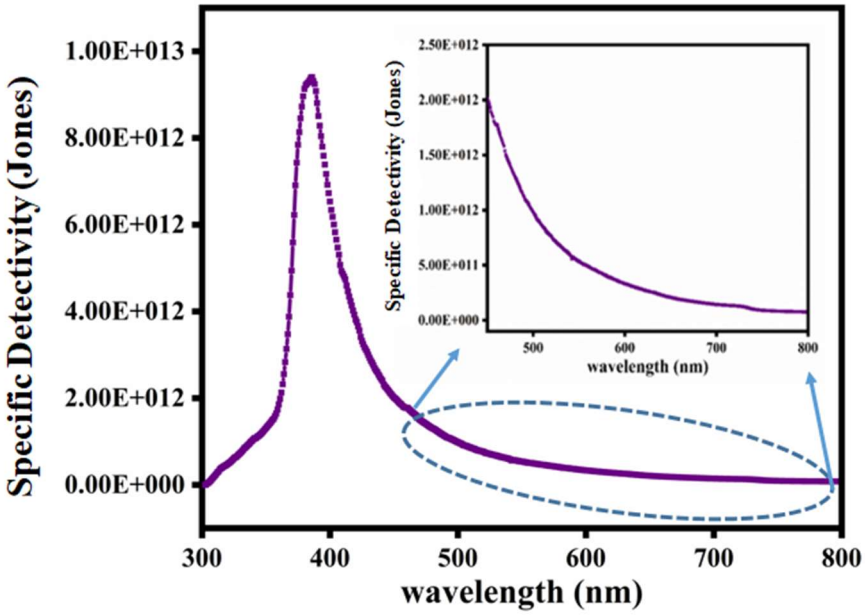

Figure 4.7 Specific Detectivity of the Fabricated Device (Inset shows enhanced performance in visible region)

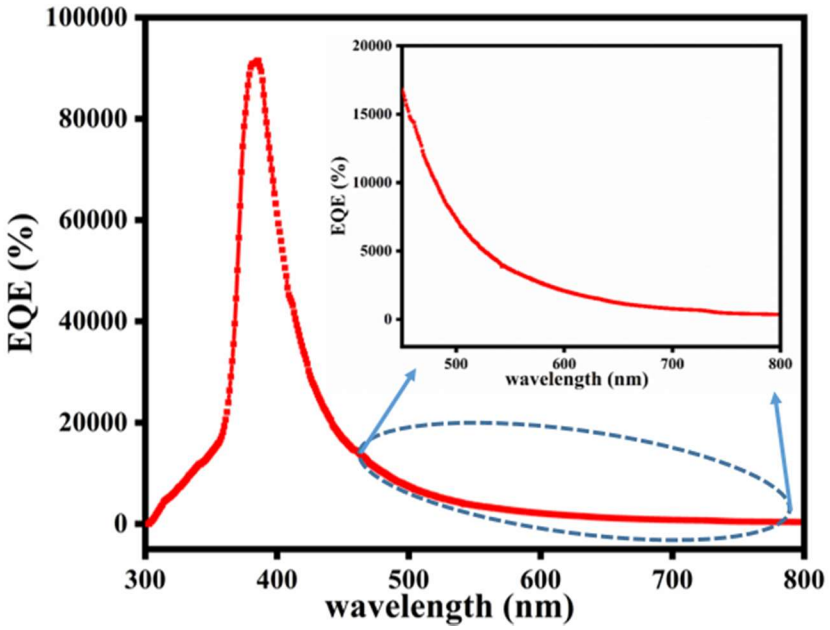

Figure 4.8 EQE of the Fabricated Device (Inset shows enhanced performance in visible region)

Figure 4.9 shows the transient response characteristics measured at room temperature of the proposed device for determining its rise time and fall time under an ON/OFF light pulse applied on the device with a bias voltage of 2 V. The rise-time (fall-time) is defined as the duration needed for current to change from 10% (90%) to 90% (10%) of its peak value. The rise time (fall time) for 380 nm estimated from **Figure 4.9** (a) and (b) is 7.25 sec (2.25 sec) while the rise time (fall time) for 550 nm estimated from **Figure 4.9** (c) and (d) is 1.2 sec (2.2 sec).

Table 4.1 shows the comparison of various performance parameters of the ZnO/TMDs based heterostructure devices. It is observed that our proposed device is better than the reported devices listed in the table.

Table 4.1 Comparison of Responsivity, Detectivity, EQE and Time response of the $MoSe_2$ based photodetectors

Device Structure	**R(λ) (A/W)**	**D(λ) (Jones)**	**EQE (%)**	**Rise time (Fall time)**	**Ref.**
ZnO QD/ monolayer MoS_2;(V_{ds}=1V)	0.084	1.05×10^{11}	-	1.5 s (1.1 s)	[67]
ZnO QD/MoS_2 thin film; (V_{bg} =30V)	2267	--	-	17.2 s (4.24 s)	[69]
MoS_2/ ZnO heterostructure; (V_{ds} =40 V)	2.7	-	-	----------	[70]
$MoSe_2$ flake/ Au-ZnO nanorod; (-2V)	0.43	3.4×10^{10}	115	1.4 s (5 s)	[55]
$MoSe_2$/ZnO heterostructure; (self- powered)	2.7	-	-	40 µs (50 µs)	[32]
ZnO/$MoSe_2$QD heterostructure; (-5 to 5 V)	1.48	93.7×10^{10}	504	2 s	[71]
ZnO CQD/ $MoSe_2$ heterostructure; (-2 to 2 V)	**282** **16.15**	**9×10^{12}** **5.37×10^{11}**	**90000** **3660**	**7.25 s (2.25 s) @ 370 nm** **1.2 s (2.2 s) @ 550 nm**	**This work**

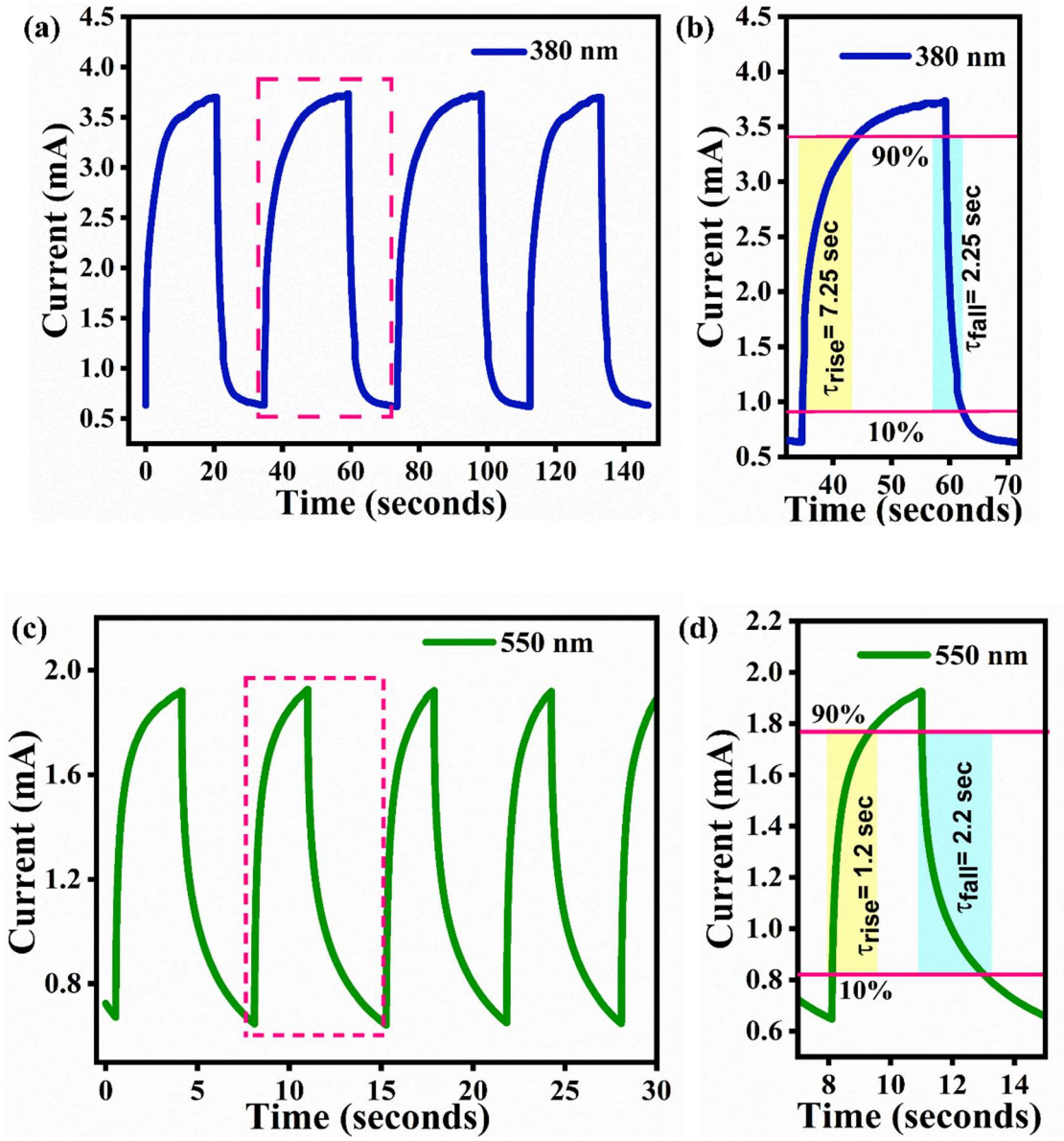

Figure 4.9 (a) Transient Response, (b) Rise (Fall) Time Calculation of the Fabricated Device at 380 nm; (c) Transient Response, (d) Rise (Fall) Time Calculation of the Fabricated Device at 550 nm.

4.4. Conclusion

The performance of a ZnO CQDs/$MoSe_2$ thin film heterojunction based UV-Visible broadband photodetector has been investigated at room temperature in this article. The proposed device gives the maximum responsivity, specific detectivity and EQE of ~282 A/W, 9×10^{12} Jones and ~90000% respectively at 380 nm (with 47 $\mu W/cm^2$ intensity) and ~16.15 A/W, ~5.37×10^{11} Jones and ~3660% at 550 nm (with 0.22 mW/cm^2 intensity) under applied bias voltage of 2 V, respectively. The rise (fall) time of the fabricated device was 7.25 sec (2.25 sec) at 370 nm illumination and 1.2 sec (2.2 sec) at 550 nm illumination under applied reverse bias voltage of 2 V. Our proposed device shows better performance than previously reported ZnO/TMDs based heterojunction devices.